Four-wave mixing in one-dimensional optical molasses

J. Guo
Joint Institute for Laboratory Astrophysics, University of Colorado, Boulder, Colorado 80309-0440
(Received 23 August 1994)

We present a detailed calculation of the four-wave-mixing signal from one-dimensional optical molasses, in which atoms are cooled by a pair of counterpropagating, cross-polarized fields. The contributions from both Raman and Rayleigh resonances between the discrete motional bound states and the recoil-induced resonances between the motional continuum states are analyzed. It is shown that the recoil-induced resonances can lead to a narrow central resonance peak in the four-wave-mixing signal with a width given by the transverse residual Doppler width. The calculated Raman sidebands also exhibit an asymmetry in the signal strength, a feature observed in recent experiments.

PACS number(s): 32.80.Pj, 42.65.−k

I. INTRODUCTION

Laser cooling is an effective way of producing extremely cold and dense samples of neutral atoms. The usual scheme of the sub-Doppler laser cooling is achieved through the so-called optical molasses, in which a pair of counter propagating, linearly polarized fields [or three pairs in three dimensions (3D)] with orthogonal polarizations are used to cool the atoms down to microkelvin temperatures. Atoms in their ground electronic states experience light shifts which are periodically modulated in space, with a modulation period determined by the optical wavelength λ. The equilibrium mean kinetic energy of the atoms in this case is smaller than the light-shift potential depth U_0. As a result, the quantized nature of the atomic center-of-mass (c.m.) motion becomes important. Evidence for the quantization of the atomic c.m. motion is provided by the observed sidebands in either the probe-transmission spectra [1–3] or the resonance fluorescence of atoms [4]. These sidebands originate from Raman transitions between the discrete motional states of atoms in the molasses, whose widths are on the order of a few tens of kHz. In the probe-transmission spectra, there also exist some extremely narrow resonance line shapes centered at zero probe-pump detuning, whose widths are typically a few kHz. Rayleigh resonances among the discrete motional states of atoms have been considered as a possible origin for these narrow signals [5]. Moreover, the so-called recoil-induced resonances [6,7], or Raman resonances between the continuum states of the atomic c.m. motion, can also lead to narrow features in the probe-transmission spectra. It has been shown [8] that the recoil-induced resonance contribution becomes the dominant source of the central resonance signal in certain pump-probe configurations.

Four-wave-mixing experiments in optical molasses have also been carried out recently in both the 1D [9] and 3D [10] cases. Due to the spatial confinement of atoms in the potential wells, enhancement of the phase-conjugating reflectivity from the molasses was observed, reminiscent of the case in semiconductor quantum wells [9]. The observed signals in these experiments exhibit similar sidebands due to Raman transitions between discrete motional states. The positions and widths of these sidebands provide information on the oscillation frequencies of the atoms in the potential wells and the damping rates of the atomic c.m. motion, respectively. There also exists an asymmetry between the strengths of the blue and red sidebands, a feature not observed in the probe-transmission experiments. A narrow central resonance peak was also observed in these four-wave-mixing experiments. A remarkable feature observed in the most recent experiment [10] is that, depending on the angle between the probe field and one of the cooling fields, the width of the central peak can be orders of magnitude smaller than the estimated relaxation rates of the discrete atomic motional states in the molasses. A smallest width of 300 Hz has been observed for the central peak in some cases.

In this paper, the four-wave-mixing signal from a 1D optical molasses is calculated to first order in the probe field strength. The internal atomic level scheme is chosen to be a $J_g = 1/2 \rightarrow J_e = 3/2$ transition. Apart from the signals originating from both the Raman and Rayleigh transitions between discrete motional states in the molasses, it is shown that, owing to the small but finite angle θ between the propagation directions of the probe and the molasses fields, the recoil-induced resonances between the transverse continuum states of the atomic motion lead to a narrow peak at zero pump-probe detuning, whose strength depends on the atomic transverse momentum spread, and whose width can be arbitrarily small, depending on the angle θ.

This paper is organized as follows. In Sec. II, the master equation for the atomic density matrix is given, and the eigenstate basis used to expand and solve this equation is described. In Secs. III and IV, we calculate the signals due to Raman and Rayleigh resonances between motional states in the optical molasses. In Sec. V, the signal due to the recoil-induced resonances is calculated, and the overall line shapes are presented. Finally, in Sec. VI, we discuss the relation of our results to some recent experiments.

II. DENSITY MATRIX EQUATION AND THE METHOD OF SOLUTION

The incident field configuration is shown in Fig. 1. The cooling fields with a frequency Ω propagate in the positive and negative $\hat{\mathbf{z}}$ directions, with polarizations in the $\hat{\mathbf{y}}$ and $\hat{\mathbf{x}}$ directions, respectively (lin$\perp$lin). The cooling fields also serve as the pump fields for four-wave mixing in this case. The probe field with a frequency Ω' propagates at an angle $\theta \in (0,\pi)$ with the $\hat{\mathbf{z}}$ direction, polarized in the $\hat{\mathbf{x}}$ direction. The total field is written as

$$\mathbf{E} = \frac{1}{2}(\mathcal{E}\hat{\mathbf{y}}e^{i\mathbf{k}\cdot\mathbf{R}-i\Omega t} + \mathcal{E}\hat{\mathbf{x}}e^{-i\mathbf{k}\cdot\mathbf{R}-i\Omega t} + \mathcal{E}'\hat{\mathbf{x}}e^{i\mathbf{k}'\cdot\mathbf{R}-i\Omega' t}) + \text{c.c.}\,, \tag{1}$$

where

$$\mathbf{k} = k\hat{\mathbf{z}},\ \mathbf{k}' = k[\hat{\mathbf{z}}\cos\theta + \hat{\mathbf{y}}\sin\theta]\,. \tag{2}$$

As in Ref. [8], we consider two limiting cases: (i) $\theta \ll 1$, which corresponds to a situation where the probe field and the nearly copropagating cooling field have orthogonal polarizations ($\aleph = \perp$); and (ii) $\theta' = \pi - \theta \ll 1$, which corresponds to a situation where the probe field and the nearly copropagating cooling field have parallel polarizations ($\aleph = \|$). In both cases, one calculates the intensity of a signal field whose frequency is $2\Omega - \Omega'$. The signal field propagates in the opposite direction to the probe field, with a polarization perpendicular to that of the probe.

As known for sub-Doppler cooling, optimal cooling effects are achieved in the limit of weak fields and large detunings, such that

$$\chi \le \Gamma \ll |\Delta|\,, \tag{3}$$

where $\chi = -d\mathcal{E}/4\sqrt{2}\hbar$ is the cooling field Rabi frequency, $d = -er_{eg}$ is a reduced atomic dipole moment, and $\Delta = \Omega - \omega$ is the detuning of the cooling field from the atomic resonance frequency ω. Under the above secular limit, the atomic excited-state populations and the electronic coherences can be adiabatically eliminated, and one obtains a master equation for the atomic ground-state density matrix only. To first order in the probe field Rabi frequency

$$\chi' = \epsilon\chi\,, \tag{4}$$

where $\epsilon \ll 1$, the equation of motion for the atomic ground-state density matrix can be written as

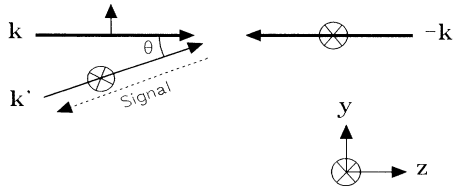

FIG. 1. Incident field configuration for four-wave mixing. The cooling (pump) fields propagate in the $\pm\mathbf{k}$ directions, and the probe field propagates in the $\mathbf{k}'$ direction. The signal field propagates in the opposite direction of the probe field.

$$\dot{\rho} = \frac{1}{i\hbar}[H,\rho] + [\dot{\rho}]_{\text{relax}}\,, \tag{5}$$

where the Hamiltonian H can be written as

$$H = H^{(0)} + \epsilon\{H^{(1)}e^{i\delta t} + [H^{(1)}]^{\dagger}e^{-i\delta t}\}\,, \tag{6}$$

in which $\delta = \Omega' - \Omega$ is the probe-pump detuning. The zeroth order Hamiltonian $H^{(0)}$ is given by

$$H^{(0)} = \frac{\mathbf{p}^2}{2M} + U_0[1 + \tfrac{1}{2}\sin(2kz)]|+\rangle\langle+| + U_0[1 - \tfrac{1}{2}\sin(2kz)]|-\rangle\langle-|\,, \tag{7}$$

which describes the motion of the atoms of mass M in the unperturbed light-shift potentials induced by the cooling fields only, with the potential depth U_0 given by

$$U_0 = \frac{8}{3}\frac{\Delta\chi^2}{(\Gamma/2)^2 + \Delta^2}\,. \tag{8}$$

The first order term $H^{(1)}$ is given by

$$H^{(1)} = \frac{U_0}{4}[-ie^{i(\mathbf{k}-\mathbf{k}')\cdot\mathbf{R}} + 2e^{-i(\mathbf{k}+\mathbf{k}')\cdot\mathbf{R}}]|+\rangle\langle+| + \frac{U_0}{4}[ie^{i(\mathbf{k}-\mathbf{k}')\cdot\mathbf{R}} + 2e^{-i(\mathbf{k}+\mathbf{k}')\cdot\mathbf{R}}]|-\rangle\langle-|\,, \tag{9}$$

which describes the modification to the potentials due to the presence of the probe field. In Eqs. (7) and (9), $|\pm\rangle$ denote the ground-state sublevels $|g,\pm 1/2\rangle$, respectively. The relaxation term $[\dot{\rho}]_{\text{relax}}$ in Eq. (5) represents the effects of optical pumping on the atomic density matrix evolution, which can be given as

$$[\dot{\rho}]_{\text{relax}} = -\frac{\Gamma'}{2}[A\rho + \rho A] + \Gamma'\int d\mathbf{p}' \sum_{Q=-1}^{1} N_Q(\mathbf{p}')B_Q^{\dagger}e^{-i\mathbf{p}'\cdot\mathbf{R}/\hbar} \times \rho e^{i\mathbf{p}'\cdot\mathbf{R}/\hbar}B_Q\,, \tag{10}$$

where $\Gamma' = \Gamma\chi^2/[(\Gamma/2)^2 + \Delta^2]$ is the optical pumping rate. The operators in Eq. (10) are given by

$$A = A^{(0)} + \epsilon\{A^{(1)}e^{i\delta t} + [A^{(1)}]^{\dagger}e^{-i\delta t}\}\,, \tag{11}$$

where

$$A^{(0)} = \tfrac{4}{3}[2 + \sin(2kz)]|+\rangle\langle+| + \tfrac{4}{3}[2 - \sin(2kz)]|-\rangle\langle-|\,, \tag{12}$$

$$A^{(1)} = \frac{2}{3}[-ie^{i(\mathbf{k}-\mathbf{k}')\cdot\mathbf{R}} + 2e^{-i(\mathbf{k}+\mathbf{k}')\cdot\mathbf{R}}]|+\rangle\langle+| + \frac{2}{3}[ie^{i(\mathbf{k}-\mathbf{k}')\cdot\mathbf{R}} + 2e^{-i(\mathbf{k}+\mathbf{k}')\cdot\mathbf{R}}]|-\rangle\langle-|\,, \tag{13}$$

and

$$B_Q = B_Q^{(0)} + \epsilon B_Q^{(1)}e^{i\delta t}\,, \tag{14}$$

where

$$B_{\pm}^{(0)} = (-ie^{-ikz} \mp e^{ikz})(|\pm\rangle\langle\pm| + \tfrac{1}{3}|\mp\rangle\langle\mp|) ,$$
$$B_0^{(0)} = \frac{\sqrt{2}}{3}(-ie^{-ikz} + e^{ikz})|+\rangle \times\langle -| + \frac{\sqrt{2}}{3}(-ie^{-ikz} - e^{ikz})|-\rangle\langle +| , \quad (15)$$

$$B_{\pm}^{(1)} = \mp e^{-i\mathbf{k}'\cdot\mathbf{R}}(|\pm\rangle\langle\pm| + \tfrac{1}{3}|\mp\rangle\langle\mp|),$$
$$B_0^{(1)} = \frac{\sqrt{2}}{3}e^{-i\mathbf{k}'\cdot\mathbf{R}}(|+\rangle\langle -| - |-\rangle\langle +|) . \quad (16)$$

The functions $N_{\pm,0}(\mathbf{p}')$ in Eq. (10) are the spontaneous photon momentum distribution functions associated with the σ ($Q = \pm$) or π ($Q = 0$) transitions. As a simplification, we assume that the spontaneous photon momentum $\mathbf{p}'$ is along the molasses direction only, i.e., $\mathbf{p}' = p'\hat{\mathbf{z}}$, and

$$N_{\pm}(p') = \frac{3}{8\hbar k}\left(1 + \frac{p'^2}{\hbar^2 k^2}\right) ,$$
$$N_0(p') = \frac{3}{4\hbar k}\left(1 - \frac{p'^2}{\hbar^2 k^2}\right) . \quad (17)$$

One can also write down the atomic ground-state density matrix ρ as

$$\rho = \rho^{(0)} + \epsilon\{\rho^{(1)}e^{i\delta t} + [\rho^{(1)}]^{\dagger}e^{-i\delta t}\} . \quad (18)$$

The four-wave-mixing signal, expressed in terms of the atomic density matrix, is found to be given by [5]

$$\xi_s = |\langle 2i\rho_s^{(1)}e^{i\mathbf{k}\cdot\mathbf{R}+i\mathbf{k}'\cdot\mathbf{R}}\rangle - \langle\rho_d^{(1)}e^{-i\mathbf{k}\cdot\mathbf{R}+i\mathbf{k}'\cdot\mathbf{R}}\rangle|^2 , \quad (19)$$

where $\langle\cdots\rangle$ denotes a spatial average, and

$$\rho_s^{(1)} = \langle +|\rho^{(1)}|+\rangle + \langle -|\rho^{(1)}|-\rangle ,$$
$$\rho_d^{(1)} = \langle +|\rho^{(1)}|+\rangle - \langle -|\rho^{(1)}|-\rangle . \quad (20)$$

$\rho_s^{(1)}$ and $\rho_d^{(1)}$ represent the probe-modulated atomic population and magnetization gratings. From Eq. (19), the components of $\rho_s^{(1)}$ and $\rho_d^{(1)}$ that contribute to the signal vary in space as $e^{-i\mathbf{k}\cdot\mathbf{R}-i\mathbf{k}'\cdot\mathbf{R}}$ and $e^{i\mathbf{k}\cdot\mathbf{R}-i\mathbf{k}'\cdot\mathbf{R}}$, respectively.

Under the secular limit (3), it is most convenient to solve Eq. (5) in the eigenstate basis of the unperturbed Hamiltonian H_0, which describes the coherent motion of atoms in the molasses fields, as well as the atomic motion in the transverse direction. The eigenstates of H_0 can be written as a product of $|n,q,\mu\rangle|p_y\rangle$, where the Bloch states $|n,q,\mu\rangle$ (n is the band index, q the Bloch index, and $\mu = \pm$) are the eigenstates of

$$H_z^{(0)} = \frac{p_z^2}{2M} + U_+^{(0)}(z)|+\rangle\langle +| + U_-^{(0)}(z)|-\rangle\langle -| \quad (21)$$

with $U_{\pm}^{(0)}(z) = U_0[1 \pm \frac{1}{2}\sin(2kz)]$, and the plane wave states $|p_y\rangle$ are the eigenstates of the free motion of the atoms in the transverse direction. The atomic motion in the x direction is irrelevant in this problem and therefore ignored. In this product basis, the atomic density matrix elements can be generally written as

$$\rho(n,q,\mu,p_y;n',q',\mu',p_y') = \langle p_y|\langle n,q,\mu|\rho|n',q',\mu'\rangle|p_y'\rangle . \quad (22)$$

The zeroth order density matrix $\rho^{(0)}$ can be solved from Eq. (5) in the absence of the probe. In the secular limit (3), one can neglect the off-diagonal density matrix elements in the Bloch state basis [11]. As a result, the only nonvanishing quantities in the Bloch-state space are the populations of various states $\pi_{n,q,\mu}^{(0)}$. The atomic momentum distribution in the direction transverse to the 1D molasses is arbitrary in our model. As in the experiment of Ref. [9], we assume that the atoms are first cooled in all three dimensions before the transverse cooling beams are switched off, and the probe beam is turned on. Therefore, the atomic momentum distribution in the transverse direction can be described by a function $W(p_y)$, whose width p_0 is on the order of a few tens of $\hbar k$, which is typical of sub-Doppler temperatures. The zeroth order atomic density matrix is thus given by

$$\rho^{(0)}(n,q,\mu,p_y;n',q',\mu',p_y') = \pi_{n,q,\mu}^{(0)}W(p_y)\delta_{n,n'}\delta_{q,q'}\delta_{\mu,\mu'}\delta(p_y - p_y') . \quad (23)$$

The values for $\pi_{n,q,\mu}^{(0)}$ are solved from Eq. (5) by setting $\epsilon = 0$. We choose the number of Bloch states up to $n = 60$, which proves to be sufficient.

As the next step, we then solve for the atomic density matrix to first order in the probe field strength, and substitute the result into Eq. (19) to calculate the four-wave-mixing signal. Similar to the case of probe transmission [8], the overall signal consists of the Raman and Rayleigh signals, which arise from stimulated Raman and Rayleigh transitions between the discrete motional states in the molasses direction. Moreover, there can be a signal originating from the recoil-induced resonances between the transverse continuum states, owing to the finite angle θ (or θ'). In the following, we calculate these various contributions, and the results are given for both the $\aleph = \perp$ and $\aleph = \parallel$ cases, respectively.

III. CALCULATION OF THE RAMAN SIGNALS

From Eq. (19), the density matrix elements representing the various Raman resonance signals have the form $\rho^{(1)}(n,q,\mu,p_y;n+m,q,\mu,p_y+\hbar k\theta)$, where $m = \pm 1, \pm 2, \cdots$. The equations for steady-state solutions of these Raman coherences are derived from Eq. (5) as

$$-\Bigg[\frac{\Gamma'}{2}(\langle n,q,\mu|A^{(0)}|n,q,\mu\rangle+\langle n+m,q,\mu|A^{(0)}|n+m,q,\mu\rangle)$$

$$+i\delta+i\omega_{n,q,\mu;n+m,q,\mu}-i\frac{kp_y\sin\theta}{M}\Bigg]\rho^{(1)}(n,q,\mu,p_y;n+m,q,\mu,p_y+\hbar k\sin\theta)$$

$$+\Gamma'\sum_{n',q',\mu'}\int dp'\sum_Q N_Q(p')\langle n,q,\mu|(B_Q^{(0)})^\dagger e^{-ip'z/\hbar}|n',q',\mu'\rangle$$

$$\times\langle n'+m,q',\mu'|e^{ip'z/\hbar}B_Q^{(0)}|n+m,q,\mu\rangle\rho^{(1)}(n',q',\mu',p_y;n'+m,q',\mu',p_y+\hbar k\theta)$$

$$=\frac{i}{\hbar}\langle n,q,\mu|H^{(1)}|n+m,q,\mu\rangle[\pi^{(0)}_{n+m,q,\mu}W(p_y+\hbar k\theta)-\pi^{(0)}_{n,q,\mu}W(p_y)]$$

$$+\frac{\Gamma'}{2}\langle n,q,\mu|A^{(1)}|n+m,q,\mu\rangle[\pi^{(0)}_{n+m,q,\mu}W(p_y+\hbar k\theta)+\pi^{(0)}_{n,q,\mu}W(p_y)]$$

$$-\Gamma'\sum_{n',q',\mu'}\int dp'\sum_Q N_Q(p')\langle n,q,\mu|(B_Q^{(0)})^\dagger e^{-ip'z/\hbar}|n',q',\mu'\rangle$$

$$\times\langle n',q',\mu'|e^{ip'z/\hbar}B_Q^{(1)}|n+m,q,\mu\rangle\pi^{(0)}_{n',q',\mu'}W(p_y)\,, \qquad (24)$$

where

$$\omega_{n,q,\mu;n+m,q,\mu}=\frac{1}{\hbar}(E_{n,q,\mu}-E_{n+m,q,\mu}) \qquad (25)$$

is the frequency difference between the Bloch states $|n,q,\mu\rangle$ and $|n+m,q,\mu\rangle$. The nonvanishing angle θ enters Eq. (24) as a residual Doppler broadening $kp_y\sin\theta/M$. Assuming that the residual Doppler width is much smaller than the relaxation rates of all the Bloch states due to optical pumping, i.e.,

$$ku\sin\theta\ll\gamma_{n,q,\mu}=\Gamma'\langle n,q,\mu|A^{(0)}|n,q,\mu\rangle\,, \qquad (26)$$

the residual Doppler broadening can be neglected as compared to $\gamma_{n,q,\mu}$. Equation (24) can then be simplified and solved after one integrates over p_y on both sides of the equation.

In Fig. 2(a) and 2(b), the Raman signals due to transitions between the Bloch states with $m=\pm1$ and ±2 are shown for the case $\aleph=\perp$, where $\theta\ll1$, and for the case $\aleph=\|$, where $\pi-\theta\ll1$, respectively. The potential depth is chosen as $U_0/E_k=-100$, where $E_k=\hbar\omega_k=\hbar^2k^2/2M$, is the atomic recoil energy, and the cooling field detuning $\Delta/\Gamma=-10$. As one can see from Fig. 2, the second order sidebands due to transitions between vibrational levels with $m=\pm2$ have much smaller amplitudes than the first order sidebands with $m=\pm1$. Moreover, the widths of the first order sidebands are much narrower than the optical pumping rate $2\Gamma'=7.5\omega_k$. These features are intimately related to the strong spatial localization of atoms in the light-induced potential wells, and can be explained in terms of the Lamb-Dicke effect for confined systems [5].

One notices from Fig. 2 that there exists a small asymmetry between the amplitudes of the blue and red sidebands. Such an asymmetry was also observed in recent four-wave-mixing experiments [9,10]. We explain the asymmetry as follows. The addition of the probe field has two effects. First, it induces stimulated Raman transitions between the vibrational levels together with the cooling fields [represented by the $H^{(1)}$ term in Eq. (9)]. Second, it modifies the relaxation rates of different vibrational levels due to optical pumping [represented by the $A^{(1)}$ and $B^{(1)}$ terms in Eqs. (13) and (16)]. The first effect leads to a contribution to the Raman signal amplitude that has different signs depending on the sign of δ, while the second effect has a contribution that is independent of the sign of δ. The interference of these two contributions results in the asymmetry between the

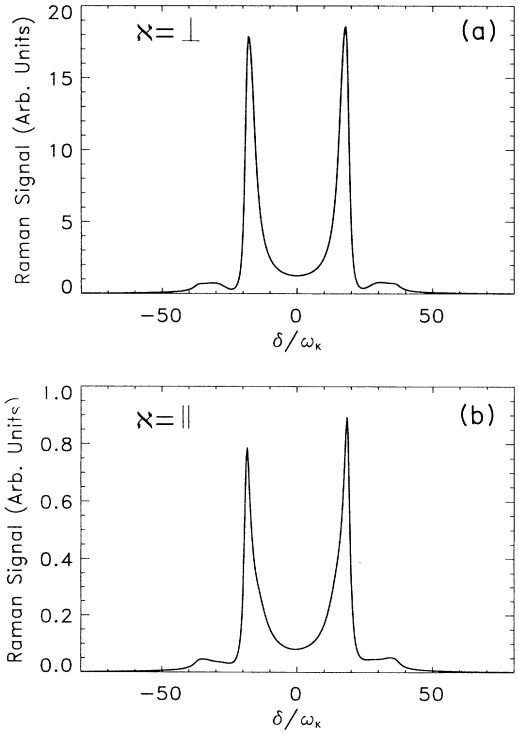

FIG. 2. Raman signals for the cases of (a) $\aleph=\perp$ and (b) $\aleph=\|$. For both cases, the potential depth $U_0=-100E_k$, and the detuning $\Delta=-10\Gamma$.

amplitudes of the blue and red sidebands, as observed in Fig. 2 [12]. We should point out that the above analysis is based on numerical evidence only. A more "physical" explanation for this asymmetry may be the subject of further investigation.

Calculations of the Raman sidebands for different values of U_0 with the same Δ indicate that the observed asymmetry has little dependence on U_0, which is understandable since the relative magnitudes of the two contributions mentioned above mainly depend on the value of $|\Delta|/\Gamma$, and the population differences between different motional states are insensitive to the value of U_0. As one increases the value of $|\Delta|/\Gamma$, the contribution due to probe-induced stimulated transitions between different motional states becomes dominant, and the asymmetry is reduced. In the limit of $|\Delta|/\Gamma = \infty$, one expects such an asymmetry to disappear.

Finally, as shown in Fig. 2, the magnitudes of the Raman signals in the two cases $\aleph = \perp$ and $\aleph = \|$ differ by about a factor of 20. As explained in Ref. [8], this is due to the particular $J_g = 1/2 \rightarrow J_e = 3/2$ transition chosen for our model. For a hyperfine transition $F \rightarrow F+1$ with $F > 1$, one expects the magnitudes of the Raman signals in these two cases to be similar.

IV. CALCULATION OF THE RAYLEIGH SIGNALS

We now calculate the signals due to Rayleigh resonances among the vibrational levels in the molasses. One can understand the Rayleigh contribution to the four-wave-mixing signal in the following scattering picture [13]. As shown in Fig. 1, there are two distinct scattering processes leading to the signal. The interference between the cross-polarized probe field and the forward pump field (propagating in the $\mathbf{k}$ direction) leads to a ground-state magnetization grating $\rho_d^{(1)}$, which varies in space and time as $\exp[i(\mathbf{k}-\mathbf{k}')\cdot\mathbf{R} + i\delta t]$. The forward scattering of the backward pump field off this grating leads to a scattered component that is polarized perpendicularly to the probe field, and propagating in the signal direction. Similarly, the interference between the parallel-polarized probe field and the backward pump field produces a population grating $\rho_s^{(1)}$ which varies as $\exp[-i(\mathbf{k}+\mathbf{k}')\cdot\mathbf{R} + i\delta t]$, and the backscattering of the forward pump field off this population grating leads to another contribution to the signal. The widths of these two contributions are determined by the relaxation rates of the respective gratings.

To calculate the Rayleigh signal, one in principle needs to include the coherences between all the Bloch states involved. Alternatively, it is more convenient to use the adiabatic state basis [5,8] in solving Eq. (5). The adiabatic states are the eigenstates of the total Hamiltonian H. In the secular limit, they can be calculated perturbatively as

$$\overline{|n,q,\mu\rangle} = |n,q,\mu\rangle + \epsilon[|n,q,\mu\rangle_+^{(1)} e^{i\delta t} + |n,q,\mu\rangle_-^{(1)} e^{-i\delta t}] , \quad (27)$$

where

$$|n,q,\mu\rangle_+^{(1)} = \sum_{n'\neq n} \frac{\langle n',q,\mu|H^{(1)}|n,q,\mu\rangle}{E_{n,q}-E_{n',q}}|n',q,\mu\rangle ,$$

$$|n,q,\mu\rangle_-^{(1)} = \sum_{n'\neq n} \frac{\langle n',q,\mu|[H^{(1)}]^\dagger|n,q,\mu\rangle}{E_{n,q}-E_{n',q}}|n',q,\mu\rangle . \quad (28)$$

The density matrix in this new adiabatic basis is diagonal, and one calculates the following matrix elements:

$$\bar{\pi}^{(1)}_{n,q,\mu}(p_y, p_y + \hbar k\sin\theta) = \langle p_y|\overline{\langle n,q,\mu|}\rho^{(1)}\overline{|n,q,\mu\rangle}|p_y + \hbar k\sin\theta\rangle , \quad (29)$$

which leads to the Rayleigh contribution to the four-wave-mixing signal. The equation for the steady-state values of $\bar{\pi}^{(1)}_{n,q,\mu}(p_y, p_y + \hbar k\sin\theta)$ can be derived from Eq. (5), which turns out to be rather complicated. It is the same as Eq. (31) of Ref. [8] for the calculation of the probe-transmission signal, and readers are referred to that paper for further reference.

Figure 3(a) shows an example of the overall Rayleigh signal in the case of $\aleph = \perp$, which is a superposition of contributions from the population grating $\rho_s^{(1)}$ (dotted line) and the magnetization grating $\rho_d^{(1)}$ (dashed line), both of which are of similar magnitudes but dif-

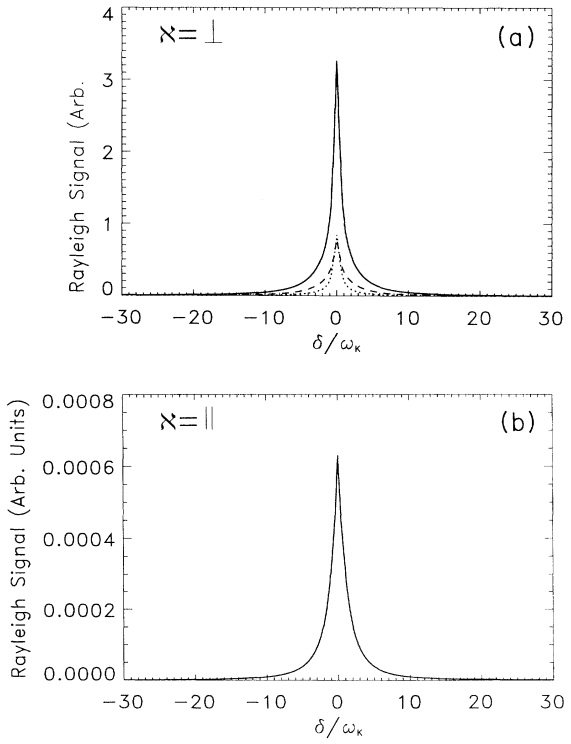

FIG. 3. Rayleigh signals for the cases of (a) $\aleph = \perp$ and (b) $\aleph = \|$. The parameters are the same as in Fig. 2. In (a), the contributions of the population grating $\rho_s^{(1)}$ and the magnetization grating $\rho_d^{(1)}$ are plotted as dotted and dashed lines, respectively.

ferent widths. In this case, one may neglect the residual Doppler broadening, similarly to the calculation of the Raman signal under the limit of Eq. (26). On the other hand, in the case of $\aleph = \|$, it is not appropriate for one to neglect the Doppler broadening. In doing so, one obtains only the contribution of the magnetization grating term $\rho_d^{(1)}$, which is shown in Fig. 3(b). The population grating term $\rho_s^{(1)}$ has zero contribution following this procedure, as is required by the population conservation condition, i.e., $\langle \rho_s^{(1)} \rangle = 0$. In fact, this procedure of calculating the contribution of $\rho_s^{(1)}$ is incorrect. As shown in the next section, the proper treatment of the $\rho_s^{(1)}$ term in the case of $\aleph = \|$ leads to the recoil-induced contribution to the four-wave-mixing signal.

V. CALCULATION OF THE RECOIL-INDUCED SIGNAL

In general, the recoil-induced resonances between the energy continuum states of the atomic motion may become important in pump-probe or four-wave-mixing spectroscopy when the temperature of atoms decreases below the Doppler limit [6]. To calculate the recoil-induced contribution to the four-wave-mixing signal in the case of $\aleph = \|$ ($\theta' = \pi - \theta \ll 1$), one needs to evaluate the coherence between atomic states with different c.m. momenta, i.e.,

$$\rho^{(1)}(p_y, p_y + \hbar k\theta') = \sum_{n,q,\mu} \bar{\pi}^{(1)}_{n,q,\mu}(p_y, p_y + \hbar k\theta') \ . \quad (30)$$

In the secular limit (3), and to lowest order in $\Gamma/|\Delta|$, the equation for $\rho^{(1)}(p_y, p_y + \hbar k\theta')$ can be derived as [8]

$$\begin{aligned} \dot{\rho}^{(1)}&(p_y, p_y + \hbar k\theta') \\ &= -\left(\gamma_t + i\delta - i\frac{kp_y\theta'}{M}\right)\rho^{(1)}(p_y, p_y + \hbar k\theta') \\ &\quad -\frac{i}{\hbar}\left[\sum_{n,q,\mu}\langle n,q,\mu|H^{(1)}|n,q,\mu\rangle \pi^{(0)}_{n,q,\mu}\right] \\ &\quad \times [W(p_y + \hbar k\theta') - W(p_y)] \ , \end{aligned} \quad (31)$$

where γ_t is an added effective decay rate, which may be determined by the transit time of atoms in the laser fields. We restrict γ_t to be smaller than any relevant frequencies in this problem, and the final results are independent of γ_t. The steady-state solution of Eq. (31) can be substituted into Eq. (19), and the recoil-induced signal is given by

$$\begin{aligned} \xi_s^{(\mathrm{RIR})} &= \left| \int dp_y \rho^{(1)}(p_y, p_y + \hbar k\theta') \right|^2 \\ &= \left| \frac{\sqrt{\pi}}{2k_BT}\left(\sum_{n,q,\mu}\langle n,q,\mu|H^{(1)}|n,q,\mu\rangle \pi^{(0)}_{n,q,\mu}\right) \right. \\ &\quad \left. \times I\left(\frac{i\gamma_t - \delta}{ku\theta'}\right)\right|^2 , \end{aligned} \quad (32)$$

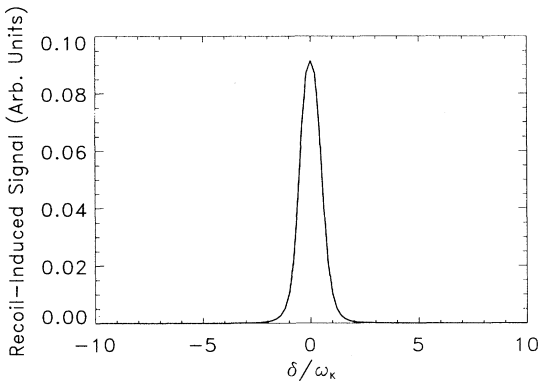

FIG. 4. The signal due to the recoil-induced resonances in the case of $\aleph = \|$. The transverse momentum spread $p_0 = 20\hbar k$, and the probe incident angle $\theta' = 1°$.

where $u = p_0/M$ is the most probable speed of atoms in the transverse direction and $k_BT = (1/2)Mu^2$ is the transverse mean kinetic energy of atoms (k_B is the Boltzmann constant). The function $I(z)$ in Eq. (32) depends on the transverse momentum distribution function $W(p)$, and is defined as

$$I(z) = \frac{i}{\sqrt{\pi}}\int_{-\infty}^{\infty}\frac{W(p_0t)p_0dt}{z-t} \ , \quad (33)$$

and $I'(z)$ is the first order derivative of $I(z)$ with respect to z. If we assume $W(p)$ to be a Gaussian, $I(z)$ becomes a tabulated function [14], with its derivative given by

$$I'(z) = \frac{2i}{\sqrt{\pi}} - 2zI(z) \ . \quad (34)$$

As one can see from Eq. (32), the recoil-induced signal is centered at $\delta = 0$, with an amplitude proportional to U_0/k_BT, and a width given by $ku\theta'$. An example of the recoil-induced signal is plotted in Fig. 4 for a Gaussian momentum distribution $W(p)$ with a width $p_0 = 20\hbar k$, and a probe incident angle $\theta' = \pi - \theta = 1°$. Comparing Fig. 3(b) and Fig. 4, one concludes that in the case of $\aleph = \|$ the recoil-induced signal has a much greater amplitude than the Rayleigh signal. The total four-wave-mixing signals for the cases of $\aleph = \perp$ and $\aleph = \|$ are displayed in Figs. 5 (a) and 5(b), respectively. In Fig. 5(a), the central peak originates from the Rayleigh contribution shown in Fig. 3(a), and its width is insensitive to the angle θ' provided that Eq. (26) holds. In the case where $kp_0 \sin\theta/M$ is comparable to or greater than the relaxation rates $\gamma_{n,q,\nu}$, both the Raman and the Rayleigh signals will be broadened by the residual Doppler width. In Fig. 5(b), the central peak is dominated by the signal due to the recoil-induced resonances, and its width varies linearly with θ'.

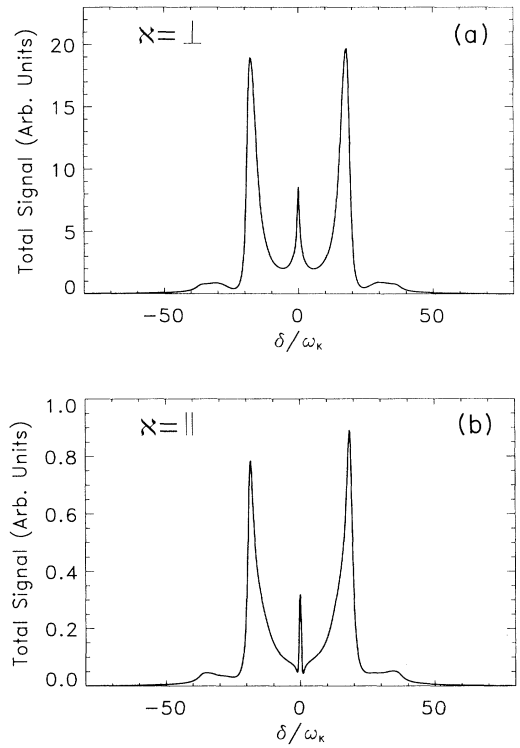

FIG. 5. Total four-wave-mixing signals for the cases of (a) $\aleph = \perp$ and (b) $\aleph = \parallel$. The parameters are the same as in Figs. 2–4.

VI. DISCUSSION

In this paper, the four-wave-mixing signal from one-dimensional optical molasses is calculated, and the different types of contributions to the signal are analyzed and compared in detail. Similarly to the probe-transmission spectra, the total signal consists of contributions from both Raman and Rayleigh resonances between the discrete atomic motional states in the molasses, as well as a recoil-induced signal originating from Raman-type resonances between the continuum states of atomic motion in the transverse direction.

The early four-wave-mixing experiment of Ref. [9] was carried out in a 1D molasses formed by a pair of counterpropagating σ^+ fields plus a constant transverse magnetic field (magnetic-assisted Sisyphus cooling). The basic features of such a molasses resemble those of a lin⊥lin molasses, and one expects that the recoil-induced signal should contribute to the central peak in the observed spectrum. A more recent experiment has been carried out in 3D optical lattices [10]. The qualitative features of the observed spectrum are quite similar to those calculated in this paper for 1D molasses. In particular, it was found in Ref. [10] that the width of the narrow central peak grows linearly with the angle between the probe and one of the cooling fields. This unique feature cannot be explained in terms of Rayleigh or Raman resonances between discrete motional states in the 3D molasses, but it is compatible with the recoil-induced signal as exhibited in this present calculation. Moreover, the smallest width of the central peak observed in Ref. [10] is nearly two orders of magnitude smaller than the estimated relaxation rates of the lowest vibrational states. In cases of 3D lattices, the degree of level degeneracy of the atomic motional states increases quadratically with energy. As a result, the atomic population in the highly excited motional states becomes significant. These highly excited states have a similar energy-momentum relation as that of free atoms, and the recoil-induced resonances associated with these continuum or quasicontinuum states may lead to a contribution to the central signals observed in both probe-transmission and four-wave-mixing experiments in 3D lattices [2,3,10]. Research along this direction is currently under way, the results of which will be reported in a planned future publication.

ACKNOWLEDGMENTS

I would like to thank A. Hemmerich for helpful discussions. I also thank J. Cooper for helpful comments. This research is supported by the E. U. Condon Fellowship Fund at JILA.

[1] P. Verkerk, B. Lounis, C. Salomon, C. Cohen-Tannoudji, J.-Y. Courtois, and G. Grynberg, Phys. Rev. Lett. **68**, 3861 (1992).
[2] G. Grynberg, B. Lounis, P. Verkerk, J.-Y. Courtois, and C. Salomon, Phys. Rev. Lett. **70**, 2249 (1993).
[3] A. Hemmerich, C. Zimmermann, and T. Hänsch, Phys. Rev. Lett. **72**, 625 (1994).
[4] P. Jessen, C. Gerz, P. D. Lett, W. D. Phillips, S. L. Rolston, R. J. C. Spreeuw, and C. I. Westbrook, Phys. Rev. Lett. **69**, 49 (1992).
[5] J.-Y. Courtois and G. Grynberg, Phys. Rev. A **46**, 7060 (1992).
[6] J. Guo, P. R. Berman, B. Dubetsky, and G. Grynberg, Phys. Rev. A **46**, 1426 (1992).
[7] J.-Y. Courtois, G. Grynberg, B. Lounis, and P. Verkerk, Phys. Rev. Lett. **72**, 3017 (1994).
[8] J. Guo, Phys. Rev. A **49**, 3934 (1994).
[9] B. Lounis, P. Verkerk, J.-Y. Courtois, C. Salomon, and G. Grynberg, Europhys. Lett. **21**, 13 (1993).
[10] A. Hemmerich, M. Weidemüller, and T. Hänsch, Europhys. Lett. **27**, 427 (1994).
[11] Y. Castin and J. Dalibard, Europhys. Lett. **14**, 761 (1991).
[12] The effects of the saturation of the optical transitions,

which are not included in our model, may also lead to an asymmetry in the sidebands [5]. However, one expects that the atoms in their internal excited states should have a negligible contribution to these narrow Raman signals.

[13] G. Grynberg, M. Vallet, and M. Pinard, Phys. Rev. Lett. **65**, 701 (1990).

[14] *Handbook of Mathematical Functions*, edited by M. Abramowitz and I. A. Stegun (Dover, New York, 1965), Chap. 7.